Computers and Concrete, *Vol. 20, No. 5 (2017) 605-616*
DOI: https://doi.org/10.12989/cac.2017.20.5.605

An experimental and numerical study on temperature gradient and thermal stress of CFST truss girders under solar radiation

Guihan Peng[1,2,3], Shozo Nakamura[2], Xinqun Zhu*[3], Qingxiong Wu[1] and Hailiang Wang[4]

[1]*School of Civil Engineering, Fuzhou University, Fuzhou, China*
[2]*Department of Civil Engineering, Nagasaki University, Nagasaki, 852-8521, Japan*
[3]*School of Computing, Engineering and Mathematics, Western Sydney University, Penrith, NSW 2751, Australia*
[4]*Tianjin Key Laboratory of Civil Structure Protection and Reinforcement, Tianjin Chengjian University, Tianjin 300384, China*

(Received July 25, 2017, Revised August 10, 2017, Accepted August 19, 2017)

Abstract. Concrete filled steel tubular (CFST) composite girder is a new type of structures for bridge constructions. The existing design codes cannot be used to predict the thermal stress in the CFST truss girder structures under solar radiation. This study is to develop the temperature gradient curves for predicting thermal stress of the structure based on field and laboratory monitoring data. An in-field testing had been carried out on Ganhaizi Bridge for over two months. Thermal couples were installed at the cross section of the CFST truss girder and the continuous data was collected every 30 minutes. A typical temperature gradient mode was then extracted by comparing temperature distributions at different times. To further verify the temperature gradient mode and investigate the evolution of temperature fields, an outdoor experiment was conducted on a 1:8 scale bridge model, which was installed with both thermal couples and strain gauges. The main factors including solar radiation and ambient temperature on the different positions were studied. Laboratory results were consistent with that from the in-field data and temperature gradient curves were obtained from the in-field and laboratory data. The relationship between the strain difference at top and bottom surfaces of the concrete deck and its corresponding temperature change was also obtained and a method based on curve fitting was proposed to predict the thermal strain under elevated temperature. The thermal stress model for CFST composite girder was derived. By the proposed model, the thermal stress was obtained from the temperature gradient curves. The results using the proposed model were agreed well with that by finite element modelling.

Keywords: temperature gradient; thermal stress; CFST composite girder; experimental study

1. Introduction

Steel-concrete composite structures have been widely used in bridge engineering due to their combination of advantages of steel and concrete. The composite structure has high strength, high ductility, and large energy-absorbing capacity (Kuranovas and Kvedaras 2007, Macorinia *et al*. 2006, Chitawadagi and Narasimhan 2009). The use of composite structures for bridges could reduce the costs and optimise the structural performance (Su *et al*. 2016). During the service period, the bridge is always subjected to thermal load induced by solar radiation and surrounding air as it exposures to the ambient environment. The temperature-induced stress can be more significant than that produced by static loads and it can cause the structural damage (Long *et al*. 2010). Zichner (1981) attributed visual cracks of concrete box-girders to the temperature variation, while the width of cracks located on the web or the bottom slab ranged from 0.2 mm to 0.4 mm. These structural cracks due to the tensile stress may subsequently grow into the large cracks that induce the rebar to be exposed to the atmosphere, and reduce the durability of the structure. Therefore, the long-term thermal load due to the temperature variations is an important factor that must be taken into account in bridge design and construction.

A literature review on thermal loads in bridges has been presented by Zhou and Yi (2013). From the review, the effect of thermal load on the performance of bridges is not fully understood and further study is needed to develop the thermal load model from the field measurement data, especially for the new type of composite bridges. Due to various thermal characteristics of different materials and the influence of the ambient temperature and solar radiation, the temperature gradient in the cross section of the composite structure is much complicated. Some numerical models have been proposed to predict the temperature gradient and thermal strain of composite girder using finite element (FE) modelling. Giussani (2009) numerically analyzed the long-term behavior of composite concrete-steel T-beams under ambient temperature. Razi and Bradford (2007) highlighted the importance of the combined actions of composite concrete-steel T-beams subjected to elevated temperatures. Shang and Liu (2012) built an FE model to analyze the thermal stress of the pre-stressed concrete box girder with corrugated steel webs and presented the calculation formulas of temperature stress. A new solar radiation model for bridge structures was proposed to include the shelter effect (Chen *et al*. 2014) and the model was verified using the field measurement data from the Tsing Ma Bridge. Westgate *et al*. (2015) studied

*Corresponding author
E-mail: xinqun.zhu@westernsydney.edu.au

ISSN: 1598-8198 (Print), 1598-818X (Online)

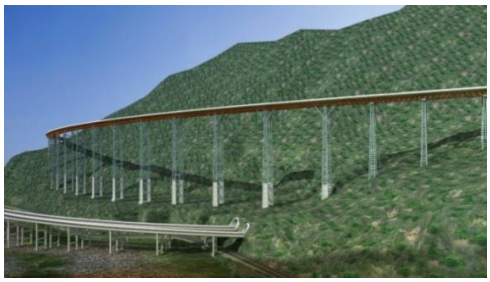

(a) Overview of the bridge

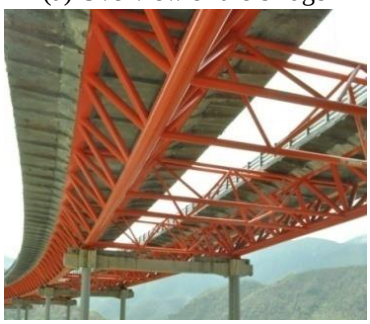

(b) The bridge truss

Fig. 1 Ganhaizi bridge

time-dependent thermal effects on suspension bridge using in-field monitored data and finite element analysis. Zhou *et al*. (2015) studied the temperature distribution of a long-span suspension bridge using numerical simulation and field measurements. The temperature gradient could cause in-plane bending of the box girder and generate the rotations at the bearings. This also affects the overturning stability of a bridge (Wang *et al*. 2016). During the construction, the thermal deformations can combine with initial imperfections and construction errors to cause the instability of the girder (Lee 2012, Kim *et al*. 2015).

To determine the thermal stress, the temperature gradient on certain cross section is needed. To compare the effects of different temperature gradient modes on the computed thermal stress, the thermal stress analysis was conducted by the researchers. Li *et al*. (2004) studied the thermal effect on Confederation Bridge using Canadian highway bridge design code and the original design temperature gradient curve. Song *et al*. (2012) studied the temperature gradients in a high-performance concrete box-girder with unconventional cross-section subjected to solar radiation. The results showed that the temperature gradient models of the current codes are not appropriate for it. Miao and Shi (2013) calculated the thermal stress of the orthotropic flat steel box girder using the measured temperature gradient, which exceeds the value from the standards, including JTG D60-2004 (MTPRC 2004) and BS5400 (BSI 2006). And the stress due to the temperature gradient according to BS5400 and EN 1991-1-5 (ECS 2003) were determined for a box girder (Mirambell *et al*. 1997). A continuous monitoring data was collected from a full-scale box-girder segment over one year and empirical formulas were developed to predict the temperature gradient of the bridge (Abid *et al*. 2016). The above studies show there is the difference in thermal-stress computed values using different temperature gradient modes from measured data or different design codes. The existing design codes cannot be used to predict the thermal stress in the CFST truss girder structures. This study is to develop the temperature gradient curves for thermal stress prediction of the structure based on field and laboratory monitoring data.

Recently, a novel type of light-weight composite bridges with CFST truss girders has been constructed and promoted in China. To authors' knowledge, there is little study on the thermal load of this CFST truss girder. The paper is to investigate the temperature gradient of the girder. Thermal couples were installed on the real bridge (Ganhaizi Bridge) for a two-month field test. The field monitoring data was used to extract the temperature gradient at the cross section of this typical bridge. In order to further investigate the thermal load of this structure, a 8:1 scale CFST truss bridge model was also built in an outdoor laboratory. An experimental study was conducted to analyze the temperature gradient and the thermal strain in the cross sections of CFST truss girder. The distribution and evolution of temperature gradient and thermal strain were analyzed from both in-field and laboratory measurements. A temperature gradient along height was obtained. The model for predicting thermal stress of this type composite girder using the temperature gradient curves was also proposed. The thermal stress predicted by the proposed model was compared with that using the finite element model.

2. Prototype structure-Ganhaizi bridge

Composite structures have been widely used in bridge constructions. Recently, a new type of CFST composite truss bridge was adopted by many bridges in China, such as the Zidong Bridge, Xiangjiaba Bridge and also Ganhaizi bridge (Zhang *et al*. 1999, Peng *et al*. 2012). Compared with traditional composite girder bridges, the solid steel girder is replaced with this CFST composite truss girder. It significantly reduces the structural weight itself and the construction difficulty in building the long span bridge, and also simplifies the substructure. The CFST composite truss girder has a light weight and the good earthquake-resistant performance. As the components of the new composite structure can be pre-casted in the factory, the construction in the field becomes easy and quick and the labor cost could be reduced. At the first stage of the construction process for the CFST truss girder, the steel skeleton, which consists of the CFST upper chord, the steel truss web and the CFST bottom chord, is launched to the accurate position. And then the concrete is poured into the top and bottom chord tubes.

The CFST composite truss girder consists of the concrete deck, the steel truss web and the upper and bottom CFST chords. When the structure is subjected to the temperature loading, the thermal stress distribution becomes very complicated due to the interaction of different components and different thermal conductivities in different materials. In this study, Ganhaizi bridge is selected as the prototype structure to conduct the research on the temperature gradient and thermal stress. As shown in Fig. 1, the Ganhaizi Bridge is located in Sichuan Province, China. Since there was a major earthquake occurred around this area, the light-weight construction is adopted for the

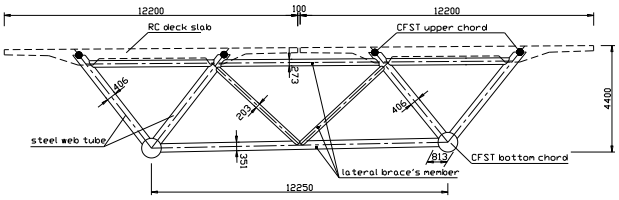

Fig. 2 Cross section of CFST truss girders (unit: mm)

Fig. 3 Weather station in the field

purpose of the good seismic performance. The total length of this bridge is 1811 m with three continuous girder units, in which the second unit is the longest one of 1044.7 m with the maximum single span of 62.5 m.

A typical CFST truss girder in this bridge is shown in Fig. 2. It comprised a concrete deck on top, a bottom CFST chord and the steel truss web members made of hollow steel tubes with a diameter of 406 mm. The width of the concrete slab is 12.2 m and its depth is 4.4 m. The thickness of the concrete deck is 50mm and it is 70 mm at the connection to web member. The web members are made of hollow steel tubes with a diameter of 406 mm and the bottom CFST chords with a steel tube of 813 mm diameter and 18 mm to 32 mm thickness that is filled with concrete. The strengths of the concrete adopted in the deck and the bottom chord is 50 MPa and 60 MPa, respectively. All the steel members employ Q345C steel plate with the yield strength of 345 MPa.

3. In-field investigation

3.1 Sensor layouts

A field testing has been carried out on Ganhaizi Bridge. The last span of the bridge with the length of 45.10 m was chosen as the test span and there is enough clearance under the bridge that can avoid the influence of the reflect radiation from the ground. Fig. 3 shows the weather station that was set-up nearby the test span. The sensors were embedded in the concrete slab when the bridge was built. Due to the good conductivity and thin thickness of the steel web member, the temperature in the whole web is considered as uniform. The temperature gradient of the CFST bottom chord is ignored.

The sensor layout is shown in Fig. 4 and the installation of thermal couples on the truss web and the concrete deck is shown in Fig. 5. 12 thermal couples were installed in the cross section at the middle of the span. Eight of them were

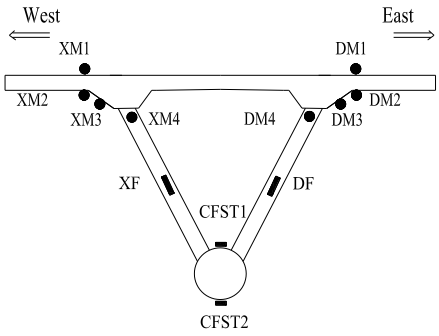

Fig. 4 Thermocouples layout on the truss girder

(a) Measurement points on the web member

(b) Measurement points on the concrete deck

Fig. 5 Installation of thermal couples

installed on the concrete deck, two sensors were on the web members and other two sensors were on the bottom chore member. In these figures, letters ‘D’ and ‘X’ refer to the east-side and the west-side of the cross-section, and ‘M’, ‘F’ and ‘CFST’ refer to the sensors on the concrete deck, the steel truss web and the CFST bottom chore, respectively.

According to the local historical weather records, the maximum air temperature difference between the morning and evening often happens in August or September every year. Hence, in order to explore the greatest cross-sectional temperature gradient, the field testing data was continuously recorded using the DH3816 temperature measurement system at a time interval of 30 minutes from 1 August 2011 to 30 September 2011.

3.2 Temperature gradient

The objective of this paper is mainly to study the vertical temperature gradient along the cross section. The term “temperature gradient” will refer to the cross-sectional temperature gradient unless specially stated in this paper. Normally the maximum temperature gradient in a whole day occurs in summer. With the sunlight movement in

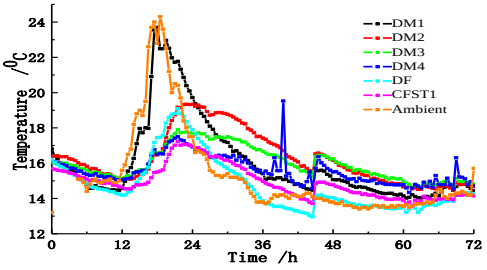

(a) Eastside sensors

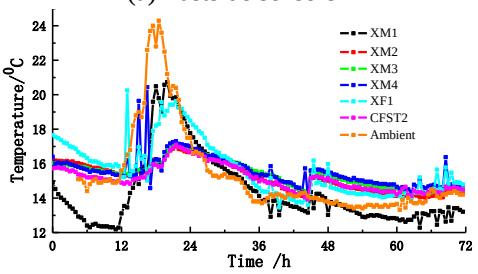

(b) Westside sensors

Fig. 6 Time-history of temperatures (1st August-3rd August: Cloudy)

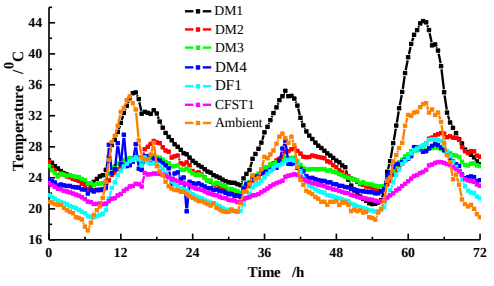

(a) Eastside sensors

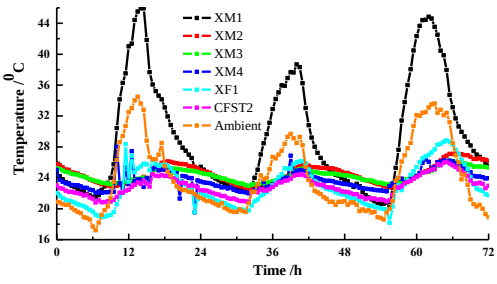

(b) Westside sensors

Fig. 7 Time-history of temperatures (15th August-17th August: Sunny)

summer, the solar radiation from a high altitude strikes horizontal surfaces, which receives much higher intensities of solar radiation than that at vertical surfaces. The temperature changes in the surrounding air and the observation points at the cross section were continuously recorded in these two months. As a typical example, Figs. 6 to 8 show the temperature time histories at observation points during three different observation periods: 1st-3rd August, 15th-17th August and 29th-31st August. 1st-3rd August were cloudy days and other days were sunny. From the results, the structural temperature and temperature gradient in cloudy days are much smaller than those in sunny days.

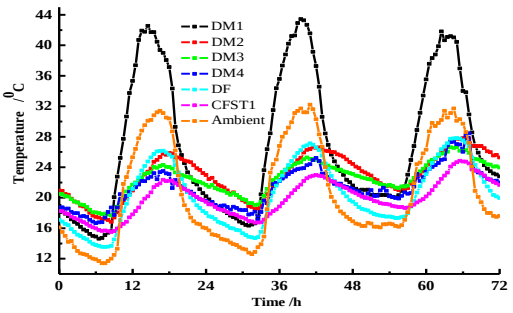

(a) Eastside sensors

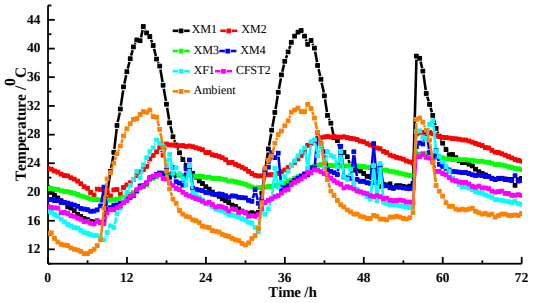

(b) Westside sensors

Fig. 8 Time-history of temperatures (29th August-31st August: Sunny)

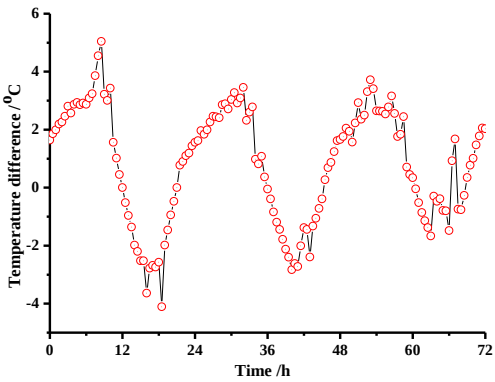

Fig. 9 Time-history of temperature difference

Compared with that in sunny days, the intensity of solar radiation in cloudy days is much small.

From Figs. 7 and 8, there are similar temperature variation patterns at the cross section under the solar radiation. The results show that the temperatures at Sensors DM1 and XM1 increase rapidly when the ambient temperature increases. DM1 and XM1 are sensor location at the east and west sides of the concrete slab respectively. Those two sensors are located at the top of the concrete slab and faced the sunlight directly. The temperatures at those two locations are increased with the solar radiation intensity increasing, and the values are much larger than that of the ambient temperature. Therefore, the solar radiation is the main factor that results in the change of temperature in this area rather than the increase of the ambient air temperature.

In Figs. 7 and 8, the temperature changes in the truss web and the bottom CFST chord under the concrete deck are much smaller than that at the top of the concrete slab. This part of the girder is mainly affected by the ambient air

Table 1 Temperature peak values at main measurement points and occurred time (unit: °C)

Location Date	DM1		DF		CFST1		Ambient air	
	Temperature	time	temperature	time	temperature	time	temperature	time
29-08-2011	42.55	14:30	26.13	16:30	22.34	17:00	31.4	16:30
30-08-2011	43.43	15:30	27.12	17:00	22.97	18:00	32.2	17:00
31-08-2011	41.82	14:30	27.78	16:30	24.85	17:30	31.7	16:30

temperature and the heat transferred from the concrete deck. Due to the weak heat conductivity of the concrete material and the shade effect provided by the concrete deck, the temperature values of these measurement points are much smaller than the ambient temperature. The concrete deck's temperature on the top reaches the peak value first due to the plenty of sunlight and there is a delay for the lowest chore members to reach their peak temperatures. Hence, the temperature gradient of the cross section is occurred.

Fig. 9 demonstrates the temperature difference at the testing points DF and DM4, which can be calculated by subtracting the temperature at DF from the temperature at DM4. DF is in the middle of the truss web and DM4 is at the bottom of the concrete deck. From the figure, affected by the hot air convection, the steel truss web can obtain the higher temperature than that of the bottom edge of the deck slab, and the maximum difference was about 4°C at the noon.

Table 1 lists the temperature peak values of the east-side testing points and they occurred during 29th-31th August 2011. The monitoring data on 29 August 2011 was used to demonstrate the evolution of temperature field and the average air temperature in that day was 19.7°C. As shown in Table 1, there is a clear time delay phenomena. The different locations reach their peak temperatures at the different time. When the top surface of the decking reaches the peak temperature, the highest temperature gradient at the cross section occurs. DM1 is at the top edge of deck slab, and its temperature increased rapidly with the intensity of solar radiation. It reaches the highest temperature of 42.6°C at 14:30. And after two hours, the ambient air obtained the highest temperature of 31.4°C at 16:30 and there was one two-hour time delay for the deck slab. Almost at the same time, the testing point DF located on the steel truss web captured the peak temperature of 26.1°C. The CFST bottom chord was the last one to attain the peak temperature of 22.3°C at 16:00 and had a half-hour delay for the truss web. It is clear that sometimes were needed for other components to obtain their highest temperature values after the top surface of deck slab had reach peak temperature. Therefore, when the top surface of the decking reached the peak temperature, the largest gradient happened and it could cause a great thermal stress and excessive displacement. With reducing the intensity of the solar radiation, the temperature value of testing points started to decrease. Specially, after the sunset, the air convection was the main factor to influence the structural temperature. The temperature difference between the measurement points decreased gradually and the temperature field returned to equilibrium. Until around 7:00 to 8:00, the deck slab, the

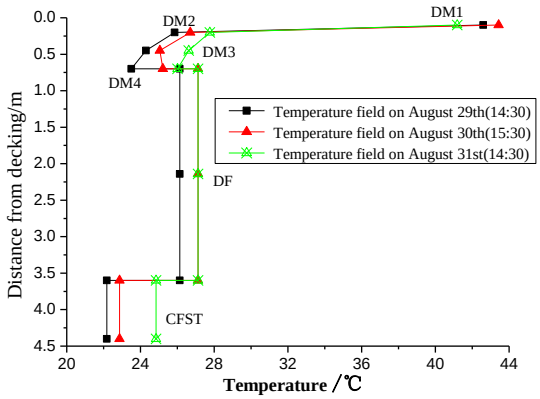

Fig. 10 Temperature gradient

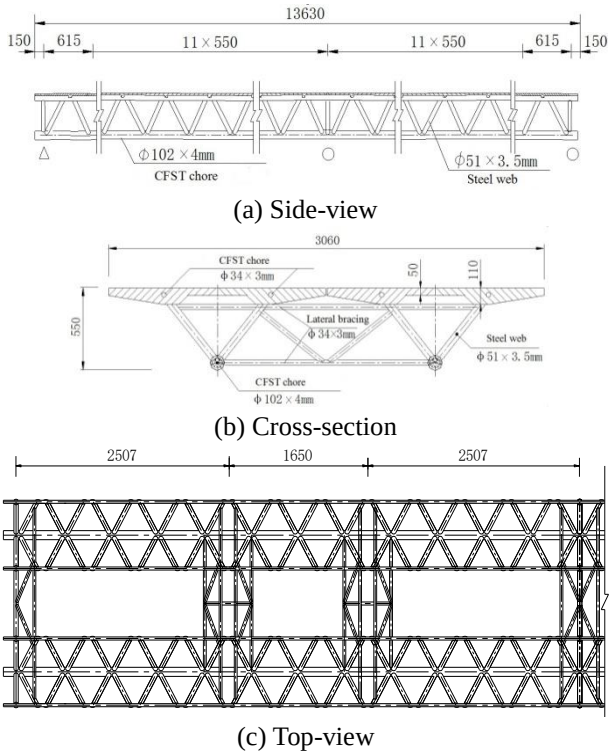

(a) Side-view

(b) Cross-section

(c) Top-view

Fig. 11 The layout of the experimental CFST truss girder (Unit: mm)

ambient air, the truss web member and the CFST bottom chord reached lowest temperature respectively. The lowest temperature values were 16.3°C, 16.7°C, 14.7°C and 12.6°C respectively.

Fig. 10 shows the temperature gradient of the cross section when the top surface of the concrete deck reaches the peak value in these three days. A multi-linear gradient mode can be obtained from the figure. The heat induced by solar radiation transferred from up to down along the depth of the cross section. Therefore, the structural temperature decreased gradually along the vertical direction of the cross section. Due to the good conductivity of steel materials and the effect of the air convection under the bridge, the steel truss web had a higher temperature than the bottom edge of concrete deck in the gradient multi-line. Thus, the temperature differences are observed at the top and bottom edges of the concrete deck, concrete deck and truss web,

(a) Steel skeleton

(b) Lashing and embedded steel bars

(c) Pouring concrete deck

(d) Laboratory model

Fig. 12 Construction stages of the 1:8 scale model

truss web and bottom CFST chord, respectively.

From the above analysis using the field monitoring data, the cross-sectional temperature gradient curve of the CFST girder has been obtained and it is mainly caused by the solar radiation. When the top surface of the bridge deck reaches the highest temperature, the structure has the biggest temperature gradient and it induces the largest thermal stress.

4. Laboratory study

4.1 Specimen

In order to further prove the correctness of the temperature fields at the cross-section of the CFST

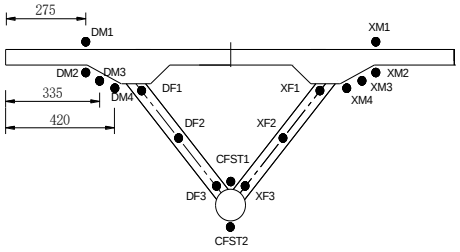

(a) Cross-section

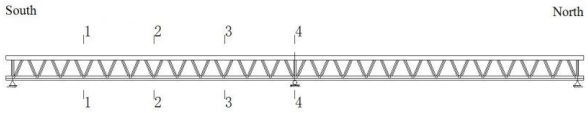

(b) Along the bridge direction

Fig. 13 Installation of thermal couples on the model (Unit: mm)

composite truss girder and analyse the temperature strain evolution, an outdoor testing had been carried out in the structural laboratory at Fuzhou University. The two-span specimen, as shown in Fig. 11, was built to simulate the continuous girder of the Ganhaizi Bridge as studied in Section 3. Due to the limitation of the test site, the scale ratio was set to be 1:8. Fig. 12 showed the construction stages of the specimen. Both the concrete and the steel used in this model had the similar strength with that in the real full-scale bridge. The total length of the model was 13.63 m, and the width and the height were set to be 3.06 m and 0.55 m, respectively. There were 12 truss units in each span with the space interval of 0.55 m. The upper and bottom chores were built with steel tubes which were stuffed by concrete and had the size of ϕ34×3 mm and ϕ102×4 mm, respectively. The size of the web that is made of the hollow steel tubes was ϕ51×3.5 mm. The average thickness of the bridge deck was 50 mm, and it was 110 mm at the connection of the deck and the web member. The composite truss girder was separated by two units along transverse direction during construction, and there was 1 mm interval between two deck flanges. Also, four lateral braces composed of the hollow steel tubes with the size of ϕ34×3 mm were set between two adjacent units to ensure a sufficient torsional stiffness.

4.2 Layout of sensors and experimental procedure

The CFST girder model was moved to the outside of the building for thermal tests after it was built. According to the layout of the real bridge, the model was set up to the north-south direction. To simulate the actual environment for the ground reflected radiation and allow the free fluent of air under the bridge, the specimen was lift from the ground using steel supports with rolling constraints, which ensure the specimen can stretch freely in the longitudinal direction. Thermal couples were installed on the specimen and the temperature data was collected using the DH2816 system every 30 minutes automatically.

To investigate the temperature distribution of truss girders, four typical cross-sections, Cross-sections 1 to 4, were selected and 96 thermal sensors were used. Among

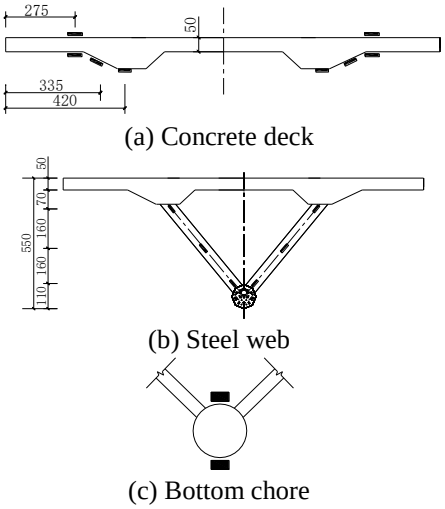

(a) Concrete deck

(b) Steel web

(c) Bottom chore

Fig. 14 Installation of Strain gauges on the deck and the truss structure (Unit: mm)

them Cross-section 2 was the middle of the span, Cross-sections 1 and 3 were at the one-quarter span and three-quarter span respectively, and Cross-section 4 was at the middle support section. 16 thermal couples were installed in each section, including eight on the deck, one each on the upper, lower ends and one in the middle of steel web member, and one each for the upper and lower chores. The detail of the sensor layout is shown in Fig. 13, in which 'D' and 'X' refer to the east-side and west-side of the cross-section, and 'M','F' and 'CFST' refer to the direction on the concrete deck, steel web and CFST chores, respectively. Strain gauges were also installed on the selected cross-section for monitoring the strain caused by temperature changes. As shown in Fig. 14, there were 16 strain gauges in total, with eight installed on the concrete deck and six on the truss web.

4.3 Temperature gradient

Thermal data as well as the strain data were collected continuously from 18th July till 16th August in 2012. There are the similar temperature distributions on the four cross-sections, which indicate the temperature field varies little along the longitudinal direction. In the following study, the monitoring data at Cross-section 2 was chosen for the detail analysis. Partial typical temperature data collected from the mid-span section is plotted in Fig. 15. The temperature field has also a clear distribution along the height of the cross section. Fig. 16 shows the typical temperature data from each test point during 31st July and 1st August in 2012. There were plenty of sunlight during these two days and the average atmospheric temperature was around 31.8℃. The highest and lowest temperatures were captured around 15:30 and 6:30, respectively. Due to expose to the direct sunlight, the temperature on the top of the concrete deck increases quickly. Because of the shade provided by flanges, an obvious temperature hysteresis happens on the measurement points underneath the concrete deck. By comparing the peak temperatures at all measurement points, the highest temperature of the concrete deck observed

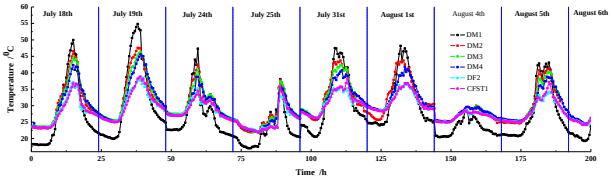

(a) East-side

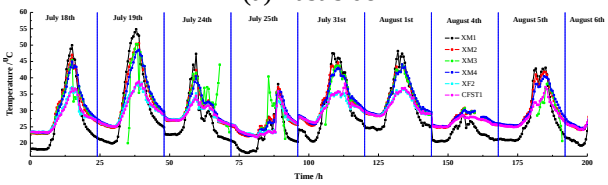

(b) West-side

Fig. 15 Temperature time-histories of test points at Cross-section 2

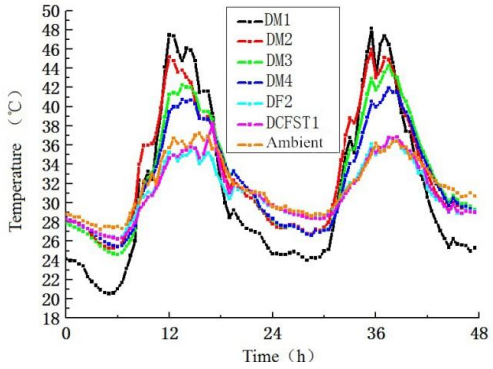

Fig. 16 Typical temperature data by eastside sensors at Cross-section 2

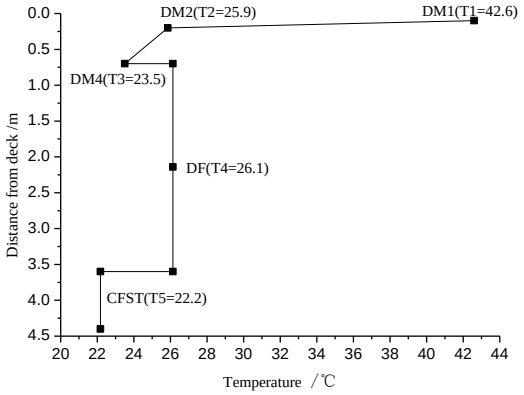

Fig. 17 The typical temperature gradient along the height of the CSFT truss girder

around 12:30, while the bottom chore reached its highest temperature around 14:00. Therefore, the most adverse temperature fields occur in this period. As the time goes by, the irradiance becomes less and the air circulation reaches balance. The deviance of the temperature distribution also reaches its minimum value.

4.4 Simplified temperature gradient curve

By further examining results at all measurement points along Cross-section 2 in the period with most severe

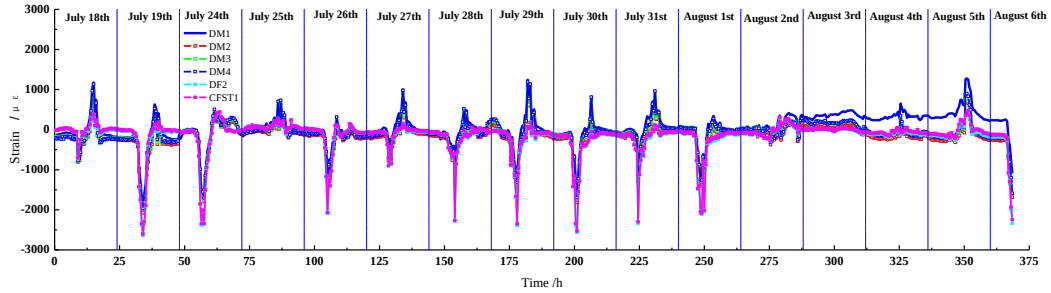

Fig. 18 Strain variations of east-side strain gauges

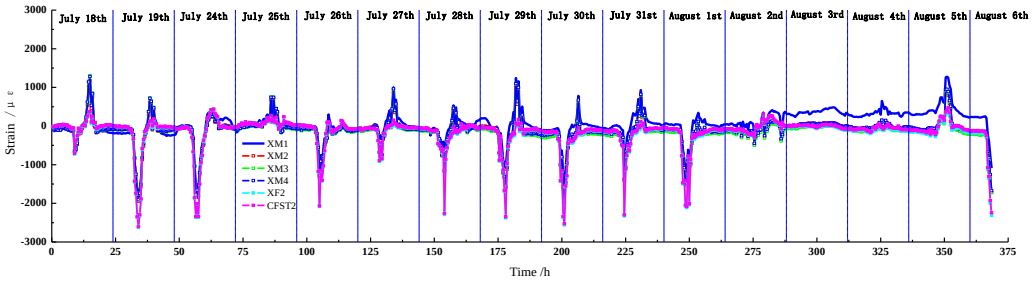

Fig. 19 Strain variations of west-side strain gauges

deviance in the temperature distribution, the temperature gradient curve can be obtained and it is shown in Fig. 17. Compared the temperature gradient curves from the full-scale bridge in Fig. 11 with that from the model at the laboratory in Fig. 17, they have the similar patterns. The critical values in the temperature gradient curve along the cross-section depend on the location, climate and the direction of the bridge structure. The values in the brackets in Fig. 17 are from the construction site when the maximum deviance on temperature distribution of the CFST truss girder occurs. At that time, the top surface of the concrete deck reaches its peak temperature.

For the concrete deck, assuming the uniformity of the material, the temperature distribution is linear inside the concrete deck. And the thickening segment at the bottom surface of the deck reflects the temperature hysteresis due to back to the sun. Meanwhile, as the concrete and the steel have different thermal conductivities, there is a sudden change at the connection point at the bottom of the deck.

For the steel truss structure, it is believed that the steel has a high conductivity. The whole part of the truss web can be assumed to have the same temperature as a straight light shown in Fig. 17.

For the CFST bottom chord which also has different thermal conductivities, a sudden change is noticed at the connection between the truss web members and the bottom chord. As the bottom chord is escaped from direct sunlight, the temperature change is mainly due to the environmental temperature. In addition, the diameter of the member is small for the CFST's conductivity. Therefore, the temperature distribution is approximate to be a straight line on the whole bottom chore part.

4.5 Thermal strains

Figs. 18 and 19 show the strain captured by the strain gauges in this period. From these figures there are similar patterns for both the strain variations at the east-side and the west-side. The thermal strain is small between 20:00 to 2:00 in the next morning. Noticed that there is no solar radiation during this time interval, and also the temperature gradient tends to reach its balance due to the strong air flow after sunset. The strain is increased between 2:00 and 6:00 and the increasing temperature gradient during this period without sunlight is also captured. The key factor on the temperature gradient is that there are different temperature changes in the concrete and steel materials due to their different thermal conductivities. After 6:00 in the morning, the sunlight radiation becomes stronger and imposes on the top of the concrete deck directly. The fast-increasing temperature on the top surface disturbs the balance and the thermal strain is induced. From the figures, the highest strain is captured around 14:00 and the temperature on the top of the concrete deck reaches its peak value. That is exactly the time when the temperature difference between the concrete deck and the steel truss web reaches the maximum value.

Due to the weak tensile strength, the stress state of concrete deck must be always paid to attention in the CFST truss girder. With the action of solar radiation, the top surface obtained much higher temperature because of facing the sunlight directly and induced much larger longitudinal expansion than that of subsequent levels in the concrete deck, especially during the noon. Thus, the uncoordinated deformation between different longitudinal fibers along the depth of the concrete deck would lead to the constraint each other, and then the thermal internal force occurred, even in simply supported spans. Normally the structural strain changed with temperature. Specially, the sensor at the top of concrete deck DM1 was the most sensitive one among all measurement points under the adequate sunlight.

Based on the experimental data in Figs. 15, 18 and 19,

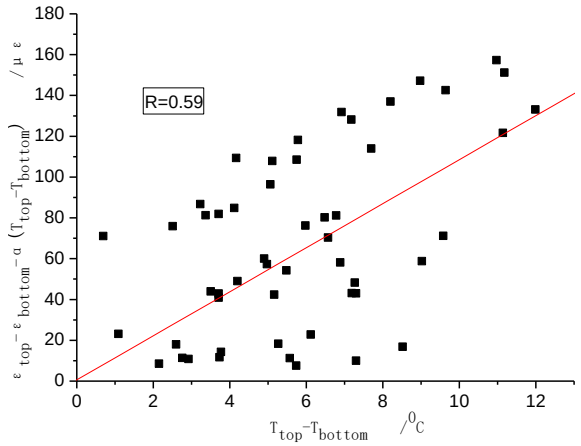

Fig. 20 Strain difference at the top and bottom surfaces of concrete deck

the strain difference of the top and bottom edge of concrete deck was approximately linear with the temperature change. The linear relationship was plotted in Fig. 20 by regression analysis and the R of correlation was 0.59. The structural strain difference between the top and bottom surface of concrete deck $\Delta\varepsilon$ can be obtained

$$\Delta\varepsilon = 10.79\Delta T + 0.616 \quad (1)$$

where $\Delta\varepsilon=\varepsilon_{top}-\varepsilon_{bottom}-\alpha_c\Delta T$, $\Delta T=T_{top}-T_{bottom}\cdot\alpha_c$ is the thermal expansion coefficient for concrete. ε and T are behalf of the structural strain and temperature respectively; the subscript "top and bottom" refer to the top and bottom surface of concrete deck respectively.

The total strain mainly includes the structural strain due to the internal force, thermal strain induced by the temperature change and the small creep and shrinkage strain. To get the structural strain, the thermal strain, $\alpha_c\Delta T$, must be eliminated from total strain. Eq. (1) can be used to predict the structural strain increment in the concrete deck when the temperature is increased and the structural condition could also be inspected and evaluated. Note that the monitoring strain data suffered from obvious discreteness due to many factors, such as the model scale, the geometry of the structure, the surrounding, the shrinkage creep and measurement error, etc. Eq. (1) should be further verified using the monitoring data from the full-scale bridge next step.

5. Thermal stress of CFST truss girder

5.1 Finite element model

As shown in the Fig. 21, a 2D finite element model with total 161 nodes and 210 elements was built to analyze the thermal behaviour of the two-span continuous truss girder using the commercial software ANSYS. In which, the Beam3 element were adapted for structural members with the same geometry size and material properties as that of the experimental model. The thermal expansion coefficients of the concrete and the steel, α_c and α_s, are 1×10^{-5}/°C and 1.2×10^{-5}/°C, respectively. And the elastic modulus of the

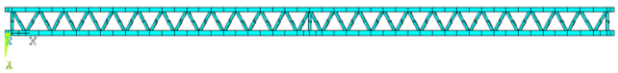

Fig. 21 Finite element model of the girder

Table 2 Temperature values

Time	Temperature values (°C)				
	D1	D4	DF	CFST	Ambient
13:30	45.25	37.55	34	33	26.7

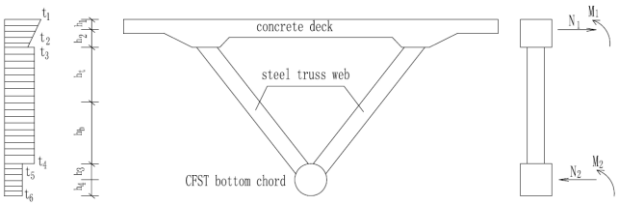

Fig. 22 Micro-segment of the CFST truss girder

concrete and the steel, E_c and E_s, are 3.45×10^{10} *MPa* and 21.0×10^{10} *MPa*, respectively. The longitudinal thermal behaviour was taken into account. As an example, the temperature field at 13:30 on 18 July 2012 was used to obtain the structural response. The details about the temperature gradient were listed in Table 2. The temperature difference between the top and bottom of the concrete deck was 7.7°C and the structural strain 73.0 $\mu\varepsilon$ was observed from the laboratory test in Section 4. It was close to the calculated value of 83.7 $\mu\varepsilon$ by Eq. (1) with the error of 12%. Eq. (1) was verified and the further research is needed to improve the accuracy.

5.2 Analytical model for thermal stress of CFST truss girders

For traditional solid web girders, the thermal stress caused by the temperature gradient could be found in articles (Ranzi and Bradford 2007, Lin 2007). However, the CFST truss girder has the different temperature distribution with the traditional girder. A new model is needed to predict the thermal stress of the CFST truss girder from temperature gradient curves.

The micro-segments of the composite truss girder are regarded as separate bodies shown in Fig. 22. As shown in Figs. 10 and 17, the temperature gradient curves have been obtained from field and laboratory monitoring data. In Fig. 22, t_1, t_2, t_3, t_4, t_5 and t_6 refer to the temperature values located on the top and bottom surfaces of the concrete deck, the truss web and CFST bottom chord, respectively. The temperature in the truss web and CFST bottom chord are assumed uniform. h_1 and h_2 are distances from the centroid of the concrete deck to its top and bottom edges, respectively. h_t and h_b are the distances between the centroid of the cross section to the bottom surface of concrete deck and the top surface of CFST bottom chord respectively. h_3 and h_4 are equal to the radius of the CFST bottom chord. The temperature t_2 is measured at the bottom of concrete deck and it depends on the heat transfer from the top of the concrete deck. The temperature t_3 is measured at the steel

truss web and it is mainly affected by the environmental air temperature. Due to the low conductivity of the concrete, t_3 is larger than t_2.

The solar radiation results in the change of the temperature field at the cross section and this induced the longitudinal deformation difference between the members, even element fibers. Due to the temperature gradient, the stress would be redistributed at the cross section. The truss web is mainly subject to shear force in the girder structure. Ignoring the contribution of the tube web to the flexural behavior of the structure, the curvature of the top concrete deck and the CFST bottom chord will be the same under the bending moments,

$$\frac{\alpha_1(t_1-t_2)}{h_1+h_2}-\frac{M_1}{E_1I_1}=\frac{\alpha_2(t_6-t_5)}{h_3+h_4}-\frac{M_2}{E_2I_2} \tag{2}$$

where M_1 and M_2 denate to the bending moments in the concrete deck and CFST bottom chord, respectively, I_1, α_1 and E_1 are the moment of inertia, the thermal expansion coefficient and the elastic modulus of the concrete deck, and I_2, α_2 and E_2 are the characteristic values of CFST bottom chord, respectively. E_2 and I_2 can be obtained as follow,

$$E_2=\frac{E_sA_{s1}+E_cA_{c1}}{A_{s1}+A_{c1}} \tag{3}$$

$$I_2=\frac{E_sI_{s1}+E_cI_{c1}}{E_s+E_c} \tag{4}$$

where A_{s1} and A_{c1} are the cross-sectional areas of the outer steel tube and in-filled concrete of the CFST bottom chord, respectively; I_{s1} and I_{c1} are their moments of inertia. The equilibrium of internal forces at the cross section can be written as

$$N_1-N_2=0 \tag{5}$$

$$M_1+M_2=N_1(h_2+h_t)+N_2(h_3+h_b) \tag{6}$$

Eqs. (2), (5) and (6) are solved simultaneously, and it can be obtained

$$M_1=\frac{E_1I_1}{E_1I_1+E_2I_2}(N_1h+\beta E_2I_2) \tag{7}$$

$$M_2=\frac{E_2I_2}{E_1I_1+E_2I_2}(N_1h-\beta E_1I_1) \tag{8}$$

where $\beta=\frac{\alpha_1(t_1-t_2)}{h_1+h_2}-\frac{\alpha_2(t_6-t_5)}{h_3+h_4}$, $h=h_2+h_b+h_t+h_3$, N_1, N_2 are axial forces at the top and bottom of the cross-section.

Assumed the construction connection is rigid, there is no slip between steel truss web and other members. At the connections between the truss web and other member, the strains due to the internal forces are equal to that by the temperature change. By this deformation compatibility condition, the following equations can be obtained,

$$\frac{N_1}{E_1A_1}+\frac{M_1}{E_1I_1}h_2=\alpha_1(t_2-t_3) \tag{9}$$

$$\frac{N_2}{E_2A_2}+\frac{M_2}{E_2I_2}h_3=\alpha_2(t_4-t_5) \tag{10}$$

By substituting Eq. (7) into Eq. (9), the internal force of the concrete deck can be obtained

$$N_1=N_2=\frac{1}{\varphi}\left[\alpha_1(t_2-t_3)-\frac{\beta E_2I_2h_2}{E_1I_1+E_2I_2}\right] \tag{11}$$

where $\varphi=\frac{1}{E_1A_1}+\frac{h\cdot h_2}{E_1I_1+E_2I_2}$.

And the stresses at the surfaces of the concrete can be obtained as

$$\sigma_{1t}=-\frac{N_1}{A_1}+\frac{M_1h_1}{I_1} \tag{12}$$

$$\sigma_{1b}=-\frac{N_1}{A_1}-\frac{M_1h_2}{I_1} \tag{13}$$

$$\sigma_{2t}=\frac{N_2}{A_2}+\frac{M_2h_2}{I_2} \tag{14}$$

$$\sigma_{2b}=-\frac{N_2}{A_2}-\frac{M_2h_2}{I_2} \tag{15}$$

where σ_{1t}, σ_{1b}, σ_{2t} and σ_{2b} denote the stresses at the top and bottom surfaces of the concrete deck and CFST bottom chord, respectively.

Table 3 shows the stress values at the top and bottom surface of the concrete deck by the proposed model and the results from the FE modelling are also listed as comparison. As the CFST bottom chord has high strength and rigidness, the stress state of the concrete deck is always a common concern due to the weak tensile strength of concrete material. In the table, the compression is positive and the tension is negative. Under the temperature gradient, the top and bottom edges of concrete deck are subject to the compressive and tensile stresses, respectively. Fig. 23 shows the stress distribution at the bottom of the concrete slab and the maximum tensile stress is around the middle support. The maximum tensile stress at the bottom edge of the concrete deck is 1.22 MPa, which is close to the result of 1.44 MPa by the finite element method. The difference of the results by the proposed method is mainly caused by neglecting the action of the truss web in the flexible behavior of the structure. As a whole, the proposed method for the thermal stress of the CFST truss girder has a good precision and a further study is needed to improve it.

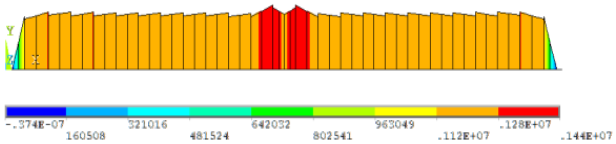

Fig. 23 The stress distribution at the bottom of the concrete deck

Table 3 Stress of the concrete deck under temperature gradient (unit: MPa)

Location method	Experimental girder		
	Top surface	Bottom surface	Strain difference
Analytical results	0.58	-1.22	62με
FE method	0.66	-1.44	73με

6. Conclusions

A two-month in-field testing and an outdoor laboratory testing were carried out for the temperature gradient of the CFST truss girder by taking the Ganhaizi Bridge as the prototype structure. The bridge is a newly constructed with the lightweight CFST truss composite girders. The evolution of the temperature gradient along the height at the cross-section has been studied using both in-field and laboratory testing data. The main conclusions can be drawn as follows: (1) The temperature gradient varies little along the longitudinal direction of the span, but there is a large change along the height of the cross-section; (2) The solar radiation is the main factor for rising the temperature on the top surface of the concrete deck, while the temperature of the steel truss member is mainly affected by the thermal conduction in the ambient condition; (3) The thermal strain has been observed from the laboratory testing, and the stain varies with the unbalance temperature field. The highest temperature strain happens when the temperature on the top surface of the concrete deck reaches its peak value; (4) As steel, concrete and CFST members have different thermal conductivities, the abrupt change of the temperature is noticed at the connections of the concrete deck to web members and the web members to the bottom chords, and attentions should be paid to this area for possible stress concentration problems.

Acknowledgments

The research described in this paper was financially supported by Technology Development Foundation of Fuzhou University (No. 2014-XQ-32).

References

Abid, S.R., Taysi, N. and Ozakca, M. (2016), "Experimental analysis of temperature gradients in concrete box-girders", *Constr. Build. Mater.*, **106**(1), 523-532.

British Standards Institution (BSI) (2006), *BS 5400-2: Steel, Concrete and Composite Bridges-Part 2: Specification for Loads*, London, U.K.

Chen, B., Sun, Y.Z., Wang, G.J. and Duan, L.Y. (2014), "Assessment on time-varying thermal loading of engineering structures based on a new solar radiation model", *Math. Prob. Eng.*

Chitawadagi, M.V. and Narasimhan, M.C. (2009), "Strength deformation behaviour of circular concrete filled steel tubes subjected to pure bending", *J. Constr. Steel Res.*, **65**(8-9), 1836-1845.

European Committee for Standardisation (2003), *EN1991-1-5: Eurocode 1: Actions on Structures-Part 1-5: General Actions-Thermal Actions.*

Giussani, F. (2009), "The effects of temperature variations on the long-term behaviour of composite steel-concrete beams", *Eng. Struct.*, **31**(10), 2392-2406.

Kim, S.H., Park, S.J., Wu, J.X. and Won, J.H. (2015), "Temperature variation in steel box girders of cable-stayed bridges during construction", *J. Constr. Steel Res.*, **112**, 80-92.

Kuranovas, A. and Kvedaras, A.K. (2007), "Behaviour of hollow concrete-filled steel tubular composite elements", *J. Civil Eng. Manage.*, **8**(2), 131-141.

Lee, J.H. (2012), "Investigation of extreme environmental conditions design thermal gradients during construction for pre-stressed concrete bridge girders", *J. Brid. Eng.*, **17**(3), 547-556.

Li, D.N., Maes, M.A. and Dilger, W.H. (2004), "Thermal design criteria for deep pre-stressed concrete girders based on data from confederation bridge", *Can. J. Civil Eng.*, **31**(5), 813-825

Lin, Y.P. (2007), *Engineers' Handbook for Bridge Design*, China Communication Press, Beijing, China.

Long, P.H., Zhang, M.H. and Chen, W.Z. (2010), "Analysis of temperature stress for concrete box girders cracking", *Proceedings of the International Conference on Mechanic Automation and Control Engineering (MACE).*

Macorinia, L., Fragiacomo, M., Amadioa, C. and Izzuddinc, B.A. (2006), "Long-term analysis of steel-concrete composite beams: FE modeling for effective width evaluation", *Eng. Struct.*, **28**(8), 1110-1121.

Miao, C.Q. and Shi, C.H. (2013), "Temperature gradient and its effect on flat steel box girder of long-span suspension bridge", *Sci. Chin. Technol. Sci.*, **56**(8), 1929-1939.

Mirambell, E. and Costa, J. (1997), "Thermal stresses in composite bridges according to BS5400 and EC1", *Proceedings of the Institution of Civil Engineers: Structures and Buildings*, **122**(3), 281-292.

Peng, G.H., Mu, T.M. and Chen, B.C. (2012), "Experimental research on flexural behavior of CFST composite truss girder", *J. Harbin Inst. Technol.*, **44**(1), 91-94.

Ranzi, G. and Bradford, M.A. (2007), "Composite beams with both longitudinal and transverse partial interaction subjected to elevated temperatures", *Eng. Struct.*, **29**(10), 2737-2750.

Shang, C.L. and Liu, W.F. (2012), "Temperature stress analysis of pre-stressed concrete box girder with corrugated steel webs", *Trans. Tianjin Univ.*, **18**, 97-103.

Song, Z.W., Xiao, J.Z. and Shen, L.M. (2012), "On temperature gradients in high-performance concrete box girder under solar radiation", *Adv. Struct. Eng.*, **15**(3), 399-415.

Su, Q., Yang, G. and Bradford, M.A. (2016), "Bearing capacity of perfobond rib shear connecters in composite girder bridges", *J. Brid. Eng.*, **21**(4), 06015009.

The Ministry of Transport of the People's Republic of China (MTPRC) (2004), *General Code for Design of Highway Bridges and Culverts*, China Communications Press, Beijing, China.

Wang, J., Xu, Z., Fan, X. and Lin, J. (2016), "Thermal effects on curved steel box girder bridges and their countermeasures", *J. Perform. Constr. Facilit.*, 04016091.

Westgate, R., Koo, K.Y. and Brownjohn, J.M.W. (2015), "Effect of solar radiation on suspension bridge performance", *J. Brid. Eng.*, **20**(5), 04014077.

Zhang, L.Y., Li, Z.S. and Cheng, M.F. (1999), *Concrete Filled Steel Tube Spatial Truss Composite Beam Structures*, China Communication Press, Beijing, China.

Zhou, G.D. and Yi, T.H. (2013), "Thermal load in large-scale bridges: A state-of-the-art review", *J. Distribut. Sens. Netw.*, **9**(12), 217983.

Zhou, L., Xia, Y., Brownjohn, J. and Koo, K. (2015), "Temperature analysis of a long-span suspension bridge based on field monitoring and numerical simulation", *J. Brid. Eng.*, **21**(1), 04015027.

Zichner, T. (1981), *Thermal Effects on Concrete Bridges*, CEB Enlarged Meeting-Commission 2-Pavia, 292-313.

HK